Science, Engineering & Education, 10, (1), 2025, 67-73

Simulation of Electron Beam Welding of Aluminium Alloy 6061 Thin Plates

Lilyana Koleva*, Asya Asenova-Robinzonova*

University of Chemical Technology and Metallurgy, 8 Kliment Ohridski Blvd., Sofia 1797, Bulgaria

Received 10 May 2025, Accepted 31 October 2025
DOI: 10.59957/see.v10.i1.2025.9

ABSTRACT

This article presents a simulation of electron beam welding of thin plates (2 to 4 mm) made of aluminium alloy 6061 using the kinetic energy of a high-velocity electron beam, which locally heats the joint area to temperatures significantly exceeding the melting point of the material. Regression models for the geometric characteristics of the molten zone (length of the molten zone, width of the molten zone, cross-sectional area of the molten zone) have been evaluated as functions of the electron beam power, welding velocity, and plate thickness. These models are used for the multi-criteria optimization of the parameters of the electron beam welding process.

Keywords: aluminium alloy 6061, electron beam welding, multi-criterial optimization, thin plates.

INTRODUCTION

Electron beam welding (EBW) is a modern method for creating permanent joints through localized melting and subsequent solidification of the material. It is widely used in industrial processes due to its ability to produce weld seams with excellent physical and mechanical properties, including strength, resistance to mechanical loads, and durability of the joints, which are achieved with minimal structural changes and negligible thermal deformations of the welded parts. EBW is characterized by exceptional precision and high efficiency in complex geometry projects and when processing materials with strict joint quality requirements, demanding minimal thermal deformations and structural changes - challenges often difficult to overcome with traditional welding methods [1].

Aluminium alloy 6061 is among the most used alloys in the fields of communications and consumer electronics. It belongs to the 6000 series, which includes aluminium, magnesium, and silicon alloys. The primary component is aluminium (around 98 %), with additional elements including 0.8 - 1.2 % magnesium, 0.4 - 0.8 % silicon, 0.15 - 0.4 % copper, 0.04 - 0.35 % chromium, as well as traces of iron, manganese, zinc, and other elements [2, 3].

This article explores the simulation of electron beam welding of thin plates (2 to 4 mm) made of

*Correspondence to: Lilyana Koleva, University of Chemical Technology and Metallurgy,8 Kliment Ohridski Blvd., Sofia 1797, Bulgaria, e-mail: sura@uctm.edu

aluminium alloy 6061 using the kinetic energy of a high-speed electron beam that locally heats the joint area to temperatures significantly exceeding the melting point of the material [4]. Regression models have been evaluated for the geometric characteristics of the molten zone: y_1 - the length of the molten zone (mm) along the x-axis, y_2 - the width of the molten zone (mm) along the y-axis, and, y_3- the cross-sectional area of the molten zone (mm^2) in the y-z plane, as functions of the electron beam power, welding velocity, and plate thickness. These models are used for the multi-criteria optimization of the parameters of the electron beam welding process.

EXPERIMENTAL

The solution of the steady-state heat balance model, involving a linear, uniformly distributed heat source moving with the beam relative to the coordinate system of the sample, during the heating of a sheet with thickness h, assumes that no phase changes occur in the sample during the process is given in Eq. (1) [4, 5]:

$$T(r,x) = \frac{P}{2\pi\lambda h} \cdot e^{-\frac{Vx}{2a}} \cdot K_0\left(\frac{Vr}{2a}\right) + T_0. \quad (1)$$

In Eq. (1) r is the radius vector from the heat source to the point under investigation, x are the coordinates in a reference frame moving with the heat source along the sample, with the axis aligned with the direction of the electron beam's motion, y is the distance from this axis, λ and a are the thermal conductivity and thermal diffusivity of the sample (where $a = \lambda/C_p\rho$, with C_p being the specific heat capacity and ρ the sample density), $K_0(V_p/2a)$ is the modified Bessel function of the second kind of zero order, P is the absorbed electron beam energy (the beam energy P_b, corrected for energy losses due to backscattered and secondary electrons), V is the welding velocity, h is the thickness of the sample, and T_0 is the initial temperature of the sample.

Simulation experiments for electron beam welding were conducted on thin plates of aluminium alloy with thicknesses ranging from 2 to 4 mm, using the Desktop Weld Optimization Software - SmartWeld in the MatLab environment [6]. The selected ranges of process parameter variation are presented in Table 1, where z_1 is the electron beam power, z_2 is the welding velocity, and $z_3$is the plate thickness.

To prevent the formation of large molten zones, the electron beam welding process (EBW) is carried out at higher welding speeds for all possible combinations of input factors.

To study the geometric characteristics of the molten zone: y_1 - length of the molten zone (mm) along the x-axis, y_2 - width of the molten zone (mm) along the y-axis, and y_3 - cross-sectional area of the molten zone (mm^2) in the x-y and y-z planes, various combinations of process parameters were used, with an optimal composite plan implemented featuring a central point. Fifteen simulation experiments were conducted using the SmartWeld program in the Matlab environment, and the resulting values for the studied geometric characteristics of the molten zone, along with the natural values z_i and the coded values x_i in the range of [-1; 1], are provided in Table 2.

Table 1. Ranges of process parameter variation.

Factor z_i	Unit of meas.	Coded values	Minimum ($z_{min,i}$)	Maximum ($z_{max,i}$)
z_1	W	x_1	600	900
z_2	mm s^{-1}	x_2	15	25
z_3	mm	x_3	2	4

RESULTS AND DISCISSION

Modelling of the geometric characteristics of the melted zone

The obtained experimental values for the investigated geometric characteristics of the melted zone, presented in Table 2, were used for evaluating regression models that describe the relationship between them and the process parameters: electron beam power x_1, welding velocity x_2 and plate thickness x_3.

Models for the coded values of the process parameters in the range [-1 to 1] were evaluated using the Eq. (2):

$$x_i = \frac{2z_i - z_{i,max} - z_{i,min}}{z_{i,max} - z_{i,min}}, \quad (2)$$

where x_1 and z_1 are the coded and natural values of the process parameters, and $z_{i,min}$ and $z_{i,max}$ are the minimum and maximum values of the experimental ranges of the factors.

The calculation of the coded values of the factors and the evaluation of the regression models was performed using the statistical software QstatLab [7]. The regression models obtained through QstatLab are presented in Table 3, where the multiple correlation coefficient R^2 (coefficient of determination), and the adjusted coefficient of determination R^2_{adj} are shown [8]. The values of both coefficients are high (close to the maximum value of 100 %), from which it can be concluded that the evaluated models are sufficiently good for predicting, investigating, and optimizing the examined geometric characteristics of the melted zone in thin plates of aluminium alloy 6061 during the electron beam welding (EBW) process.

Figs. 1 - 3 show contour diagrams depicting the dependency of the weld pool length - y_1 (mm), weld pool width - y_2 (mm) and the cross-sectional area of the weld pool - y_3 (mm^2) on the variation of process parameters during electron beam

Table 2. Experimental plan in coded and natural values and values of the studied geometric characteristics of the molten zone in electron beam welding of thin plates of aluminium alloy.

No	Coded values			Natural values			Geometry of the molten zone		
	x_1	x_2	x_3	z_1	z_2	z_3	y_1	y_2	y_3
1	-1	-1	-1	600	15	2	2.28	2.22	4.44
2	1	-1	-1	900	15	2	7.07	6.4	12.8
3	-1	1	-1	600	25	2	1.37	1.33	2.66
4	1	1	-1	900	25	2	4.24	3.84	7.68
5	-1	-1	1	600	15	4	0.108	0.108	0.431
6	1	-1	1	900	15	4	0.808	0.803	3.21
7	-1	1	1	600	25	4	0.0647	0.0647	0.259
8	1	1	1	900	25	4	0.485	0.482	1.93
9	0	0	0	750	20	3	0.912	0.903	2.71
10	-1	0	0	600	20	3	0.365	0.364	1.09
11	1	0	0	900	20	3	1.71	1.66	4.99
12	0	-1	0	750	15	3	1.22	1.2	4.44
13	0	1	0	750	25	3	0.73	0.722	12.8
14	0	0	-1	750	20	2	3.3	3.11	2.66
15	0	0	1	750	20	4	0.27	0.269	7.68

Table 3. Regression models for the geometric characteristics of the melted zone during the EBW.

Param.	Regression model	R^2, %	R^2_{adj}, %
y_1	$0.9874 + 1.01253x_1 - 0.45963x_2 - 1.65243x_3 + 1.01217x_3x_3 + + 0.4217125x_2x_3 - 0.8174625x_1x_3$	0.9704	0.9483
y_2	$0.9698 + 0.90983x_1 - 0.42923x_2 - 1.51733x_3 + 0.89287x_3x_3 + +0.3857125x_2x_3 - 0.6972125x_1x_3$	0.9742	0.9548
y_3	$2.914 + 2.173x_1 - 0.9792x_2 - 2.69x_3 + 1.158x_3x_3 - 0.556x_1x_2 + +0.681x_2x_3 - 1.11625x_1x_3$	0.9904	0.9807

welding: electron beam power - z_1 and welding velocity - z_2.

From Figs. 1 - 3, it can generally be concluded that as the electron beam power increases, the dimensions of the melt pool increase as well, and conversely, an increase in welding velocity leads to a decrease in the melt pool dimensions.

Fig. 1 shows that the minimum values of the melt pool length are obtained for electron beam power values of $z_1 < 620$ W and welding velocity $z_2 > 24$ mm s^{-1}. Maximum melt pool lengths are achieved at welding velocities $z_2 < 16$ mm s^{-1} and electron beam power $z_1 > 860$ W.

Fig. 2 shows that the minimum values of the melt pool width are obtained at the minimum values of electron beam power $z_1 < 620$ W and welding velocity $z_2 > 24$ mm s^{-1}, while the maximum melt pool widths occur at welding velocities $z_2 < 17$ mm s^{-1} and electron beam power $z_1 > 840$ W.

Fig. 3 shows that the minimum values of the melt pool cross-sectional area are obtained at the minimum values of electron beam power $z_1 < 620$ W and welding velocity $z_2 > 22$ mm s^{-1}, while the maximum values of the melt pool cross-sectional area occur at the maximum values of electron beam power $z_1 > 860$ W and welding velocity $z_2 < 16$ mm s^{-1}.

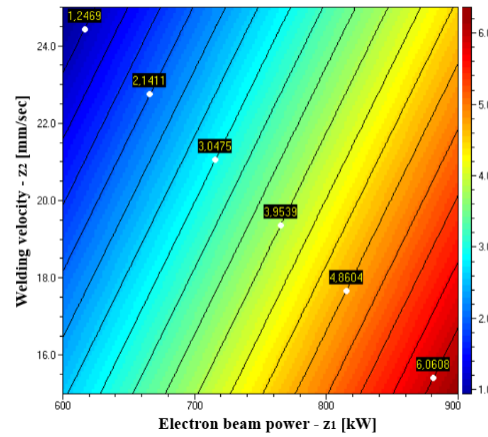

Fig. 1. Contour plot of the melt pool length - y_1 (mm) as a function of electron beam power - z_1 and welding velocity - z_2 at a plate thickness of $z_3 = 2$ mm.

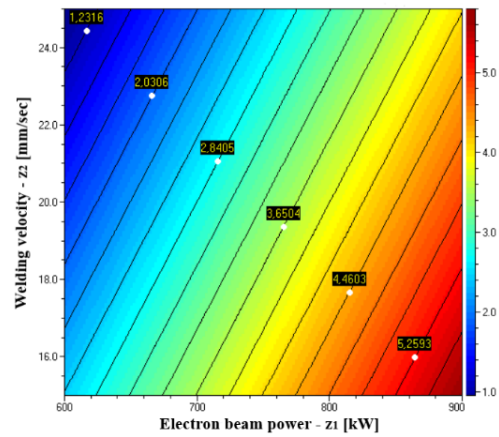

Fig. 2. Contour plot of the melt pool width - y_2 (mm) as a function of electron beam power - z_1 and welding velocity - z_2 at a plate thickness of $z_3 = 2$ mm.

Multi-criteria optimization

In multi-criteria optimization tasks, the concept of Pareto optimality has been applied

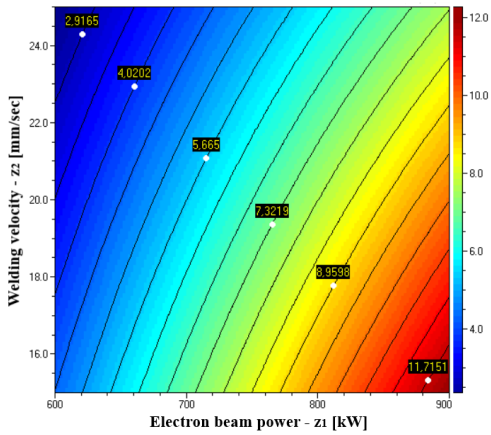

Fig. 3. Contour plot of the cross-sectional area of the melt pool - y_3 (mm^2) as a function of electron beam power - z_1 and welding velocity - z_2 at a plate thickness of z_3 = 2 mm.

according to the Pareto principle. A Pareto-optimal solution possesses the property that any deviation from it results in the deterioration of at least one of the considered criteria. The characteristic feature of Pareto-optimal solutions is that no other solution exists in the feasible domain where all components of the vector criterion $Q_j(x)$, j = 1,2,...,n have better values than the Pareto-optimal solutions.

Pareto optimization is applied to find such compromise solutions that simultaneously meet the following requirements:

- $y_1 \rightarrow$ minimum;
- $y_2 \rightarrow$ minimum;
- $y_3 \rightarrow$ minimum.

The Pareto-optimal solutions were obtained (50 solutions) by applying a genetic algorithm using the statistical software QstatLab. Each proposed solution, to some extent, makes a certain compromise in terms of quality, as any deviation aimed at improving one or more criteria leads to the deterioration of at least one of the remaining criteria. When comparing two randomly chosen Pareto-optimal solutions, some of the quality characteristics may have better values, but at least one will be worse.

A sample of the first six evaluated Pareto-optimal solutions, also referred to as the Pareto front, is presented in Table 4. When these compromise solutions are compared pairwise, it can be observed that some of the obtained optimal values are better, but at least one value is worse than in another compromise solution.

From the results shown in Table 4, it can be observed that the obtained Pareto front is very narrow, and the geometry of the resulting melt pool depends primarily on the thickness of the aluminium alloy 6061 plates - z_3. It is also evident

Table 4. Pareto-optimal solutions for process parameters and melt pool geometry characteristics.

No	z_1	z_2	z_3	$\hat{y}_1$	$\hat{y}_2$	$\hat{y}_3$
1	608.8661	25.0000	3.9187	0.0053	0.0011	0.5099
2	600.0141	25.0000	3.9315	0.0085	0.0008	0.4910
3	613.5611	25.0000	3.9121	0.0045	0.0021	0.5211
4	600.3892	25.0000	9.9303	0.0075	0.0001	0.4910
5	600.0357	15.9426	3.8063	0.0568	0.0752	0.1232
6	600.0011	22.1262	3.8924	0.0004	0.0030	0.3373
7	600.0007	15.0000	3.7770	0.0691	0.0913	0.1114
8	600.0028	21.3146	3.8797	0.0003	0.0058	0.2990
9	600.0005	15.0019	3.9032	0.1252	0.1285	0.0724
10	600.0080	15.7563	3.8072	0.0616	0.0798	0.1179

that the maximum values for the melt pool length (y_1) and width (y_2) will be obtained for regime No. 9, where the cross-sectional area of the melt pool is the smallest. The largest cross-sectional area of the melt pool (y_3) is given by Pareto front No. 5, while the maximum values for both the length and width of the melt pool will be achieved in regimes No. 8 and No. 4, respectively. The choice between some of these solutions is typically made by adding additional criteria or based on expert judgment, depending on the formulated technological requirements.

CONCLUSIONS

This article examines the simulation of electron beam welding of thin plates of aluminium alloy 6061 using the kinetic energy of a fast-moving electron beam, which locally heats the joint area to temperatures significantly exceeding the melting point of the material. The goal is to investigate the effect of variations in the input parameters: electron beam power, welding velocity, and plate thickness on the geometric characteristics of the melt pool: melt pool length (y_1), melt pool width (y_2), and melt pool cross-sectional area (y_3). An optimal composite design plan was implemented with one additional point to study this influence, and regression models for the geometric characteristics of the melt pool were evaluated.

The evaluated models were used for multi-criteria Pareto optimization through the application of a genetic algorithm, resulting in fifty Pareto-optimal solutions (regions and optimal modes) for the process parameters, with specific requirements set for the geometry of the welded samples.

When validating the obtained optimal modes, deviations between real experiments and simulated experiments can be observed. Possible causes for this may include: the heat model used in the simulation, errors in the process parameters in electron beam welding, or unaccounted noise factors (such as the position of the focus relative to the sample surface), and so on. Other heat models can also be applied, and the thermal dependence of the thermophysical properties of the aluminium alloy 6061 can be considered to improve the accuracy of the simulation. Regardless, the obtained results can be used as an initial setup for the process parameters in electron beam welding of thin aluminium alloy 6061 plates, given specific technological requirements.

After experimental validation, model adjustments (if necessary), and tuning of the process parameters, the obtained optimal modes can be used in production conditions.

Acknowledgment

The research was supported by a project funded by the European Union – NextGenerationEU through the National Recovery and Resilience Plan of the Republic of Bulgaria, project No. BG-RRP-2.004-0002, "BiOrgaMCT", and as part of contract №: BG16RFPR002-1.002-0009-C01, project name: 'Regional Centre for Digital Solutions and Innovation NCIZ', under Procedure BG16RFPR002-1.002 - Funding of selected by the European Commission European Digital Innovation Hubs awarded with Seal of Excellence, funded by Operational Programme 'Research, Innovation and Digitalisation for Smart Transformation'.

REFERENCES

1. G.M. Mladenov, E.G. Koleva, K.Zh. Vutova. Electron lithograpy of submicron- and nano-structures. Practical Aspects and Applications of Electron Beam Irradiation Transworld Research Network, India, Editors: Monica R. Nemtanu and Mirela Brasoveanu, 2011, 135-166.
2. https://www.matweb.com/search/datasheet.aspx?MatGUID=b8d536e0b9b54bd7b69e4124d8f1d20a&ckck=1
3. P. Kumar, A. Arif, A.C.V.S. Prasad, P. Danaiah, A.K. Singh, M. Patro, K S. Kishore, M. Murugan. Study of welding process parameter in TIG joining of aluminum alloy

(6061). Materials Today: Proceedings, 2021, 47, 4020-4025.
4. G. Mladenov, E. Koleva, K. Vutova. Heat Transfer and Weld Geometry at Electron Beam Welding. International Review of Mechanical Engineering (I.RE.M.E.), 5, 2, 2011, 235-243.
5. D. Rosenthal, The Theory of Moving Sources of Heat and Its Application to Metal Treatments, Transactions of the ASME, 1946, 849-866.
6. Desktop Weld Optimization Software for automated welding home page SmartWeld - http://smartweld.sourceforge.net/
7. QstatLab home page: http://www.qstatlab.co.uk/eng/index.html
8. E. Koleva, Applied Statistics. Ed. I. Vuchkov, UCTM, 2020, (in Bulgarian).